Scattering-path analysis and magnetic scattering properties of Fe/Ag(100) films: A temperature-dependent magnetic EXAFS study

J. Kurde, N. Ponpandian, J. Luo, C. Weis, and K. Baberschke
Institut für Experimentalphysik, Freie Universität Berlin, Arnimallee 14, D-14195 Berlin-Dahlem, Germany

P. Srivastava* and H. Wende†
Fachbereich Physik, Universität Duisburg-Essen, Lotharstraße 1, D-47048 Duisburg, Germany
(Received 11 July 2007; revised manuscript received 19 September 2007; published 19 December 2007)

Magnetic extended x-ray absorption fine structure (MEXAFS) is the spin-dependent counterpart of the well established extended x-ray absorption fine structure (EXAFS) technique. By means of MEXAFS, it is not only possible to analyze the local magnetic structure but also to probe magnetic fluctuations. For a fundamental understanding of this technique, we studied bulklike Fe films on a Ag(100) single crystal substrate by comparing the experimental data to *ab initio* calculations. The measurements were carried out at different temperatures. To model the temperature dependence, originating from lattice vibrations and spin fluctuations, the rigid band model was applied. The present study enables us to understand the differences in the fine structure of spin-averaged and magnetic EXAFS, to identify the scattering paths contributing to the EXAFS signal, and to reproduce the experimental spectra even with a simple rigid band model separating spin fluctuations from lattice vibrations.

DOI: 10.1103/PhysRevB.76.224418 PACS number(s): 61.10.Ht, 73.50.Bk

I. INTRODUCTION

Studies providing information related to local dynamic disorder and magnetic ordering are of immense interest, particularly for systems that show magnetic phase transitions. X-ray absorption spectroscopy in the extended energy range using linear and circularly polarized light has become the technique of choice to draw such kind of information.[1–9] The temperature dependences of extended x-ray absorption fine structure (EXAFS) and magnetic extended x-ray absorption fine structure (MEXAFS) yield the local dynamic disorder (lattice vibrations) and magnetic disorder (spin fluctuations). For systems containing 3*d* elements, measurements at their $L_{2,3}$ edges are of relevance since, thereby, the important 3*d* states can be probed. In the past, we have conclusively established that the overlap between L_2 and L_3 edges can be described accurately by *ab initio* calculations.[10,11] Furthermore, a procedure to deconvolute the experimental spectra into their L_3 and L_2 edge contributions was developed,[11] which enabled us to study higher order spin-spin correlations.

In this work, we present high quality EXAFS and MEXAFS spectra at the $L_{2,3}$ edges of a Fe bcc film of 13 ML (monolayers) on Ag(100). This is a common system with respect to its magnetic and structural properties (see, e.g., Refs. 12 and 13). The Ag substrate was chosen since no other absorption edges of the substrate are found in the Fe (M)EXAFS range. As the regular EXAFS is automatically recorded when measuring magnetic EXAFS, an attempt is made to directly compare structural properties with the local magnetic structure. A detailed scattering-path analysis including paths with an effective path length $R_{\mathrm{eff}}=5$ Å is done for this Fe bcc lattice. The rigid band model was applied here to model the temperature-dependent fine structure of the experimental 3*d*-metal MEXAFS including the respective Fourier transforms. This is crucial in order to disentangle spin fluctuations from lattice vibrations, both contributing to the damping of the MEXAFS signal. This will be important for future studies of the local spin correlations close to the Curie temperature in two dimensional Fe films.

II. EXPERIMENT AND ANALYSIS

The Fe films (13 ML) were prepared and measured *in situ* (base pressure $p \leqslant 3\times10^{-10}$ mbar). The Ag single crystal was cleaned by repeated cycles of sputtering with Ar^+ atoms (0.5 keV) and subsequent annealing (850 K). The cleanliness and the long-range order were checked with Auger electron spectroscopy and low energy electron diffraction, respectively. The films were grown at room temperature by electron beam evaporation with a rate of typically about 0.5 ML/min.

The absorption spectra were recorded at the helical undulator beamline UE56/1-PGM of BESSY using the total electron yield. The degree of circular polarized light in the EXAFS range of the Fe $L_{2,3}$ edges was about 90%. All measurements were carried out in the presence of a magnetic field ($B=18$ mT) for two different temperatures ($T=300$ and 80 K). This field is sufficient to magnetically saturate the Fe film. Since the easy axis of the sample magnetization lies in plane, we measured at grazing incidence of $\phi=20°$ to the surface plane. The absorption spectra were recorded in an energy range of $E=690-1300$ eV. In the upper part of Fig. 1, the spin-averaged absorption for $T=80$ K is shown. The spectrum is normalized to the signal to background ratio (edge jump J_R). The EXAFS signal is about 10% of the edge jump. The lower part of Fig. 1 shows the corresponding magnetic absorption. In comparison to the near edge x-ray magnetic circular dichroism signal, the amplitude of the MEXAFS oscillation is much smaller (about 1.2% of the edge jump). For clearer representation it is magnified by a factor of 100 in Fig. 1.

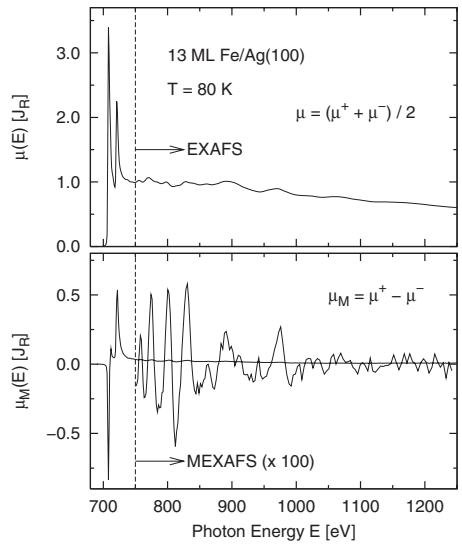

FIG. 1. Experimental EXAFS and MEXAFS spectra $\mu(E)$ and $\mu_M(E)$ at $T=80$ K. The spectra are normalized to the signal to background ratio.

The EXAFS signal $\chi(E)$ is due to Coulomb scattering of the photoelectron at the surrounding atoms. Depending on the photoelectron energy, there is constructive or destructive interference between the outgoing and backscattered electron waves. The conventional way of EXAFS analysis is to extract the oscillatory part $\chi(k)$ from the original absorption spectra according to $\chi(k)=[\mu(k)-\mu_0(k)]/J_R$, where μ_0 is the so-called atomic background and $k=\sqrt{2m_e(E-E_0)/\hbar^2}$ the photoelectron wave number. To determine the atomic background function, the AUTOBK code[14] was used. The experimental $\chi(k)$ can be described as a superposition of all scattering shells j, where each shell contributes according to

$$k\chi(k) = \sum_j N_j A_0(k,T) F(k) \frac{\sin[2kR_j + \delta(k)]}{R_j^2}. \qquad (1)$$

Here, N_j and R_j are the number and distance of atoms in the shell, $F(k)$ and $\delta(k)$ are the scattering amplitude and phase, and $A_0(k,T)$ is a damping factor including the EXAFS-Debye-Waller factor $\exp(-2\sigma^2k^2)$, where σ^2 is the mean square relative displacement of the scattering atoms due to lattice vibrations. Commonly, $\chi(k)$ is Fourier transformed into real space with R as the distance between the absorbing atom and the various backscattering atoms [shifted by the scattering phase shift $\delta(k)$]. In other words, the Fourier transform (FT) of the EXAFS oscillations is related to the radial pair distribution functions of each scattering shell.

For the MEXAFS studies, circularly polarized x-rays are used. So the photoelectrons carry a spin polarization $\langle\sigma_z\rangle$. This leads, in addition to the Coulomb potential, to an exchange interaction. The scattering amplitude for a photoelectron with spin parallel (+) and antiparallel (−) to the sample magnetization is then given by the EXAFS scattering amplitude F_C plus an additional magnetic contribution $\langle\sigma_z\rangle F_M$. For a multiple scattering process, the scattering amplitude is given by the product of the separate scattering events. Having n identical atoms, the product reduces to the power of n,[5,15]

$$F^{\pm} = (F_C \pm \langle\sigma_z\rangle F_M)^n \approx F_C^n \left(1 \pm n\langle\sigma_z\rangle \frac{F_M}{F_C}\right). \qquad (2)$$

The approximation is derived from potential series. Hence, for MEXAFS, the multiple scattering paths will be enhanced by the factor n of the scattering events.

III. RESULTS AND DISCUSSION

One main purpose of the present investigation is to study the scattering paths of the photoelectron (originating from a $2p$ state) in real space and the influence of normal potential (Coulomb) and spin-resolved (exchange) scattering on these paths. This is of interest to understand the magnetism of ultrathin ferromagnetic Fe films.

In Fig. 2, the normalized EXAFS $[\chi(k)]$ and MEXAFS $[\chi_M(k)]$ oscillations measured at 80 and 300 K and their corresponding Fourier transforms are shown. In $\chi_M(k)$, the relative amplitude in the range of the "high frequency" oscillation at $k<6$ Å^{-1} is significantly larger than in $\chi(k)$. This is

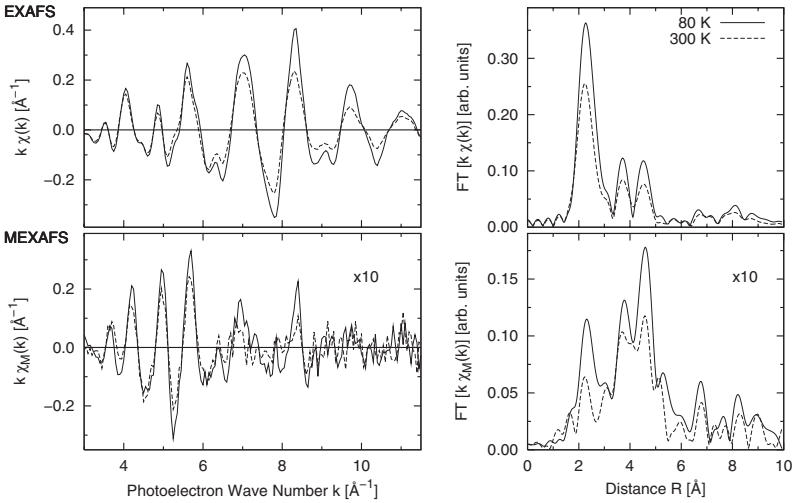

FIG. 2. Experimental oscillations $\chi(k)$ and $\chi_M(k)$ of EXAFS and MEXAFS recorded at 80 and 300 K (left). The corresponding Fourier transforms (FTs) are shown on the right hand side.

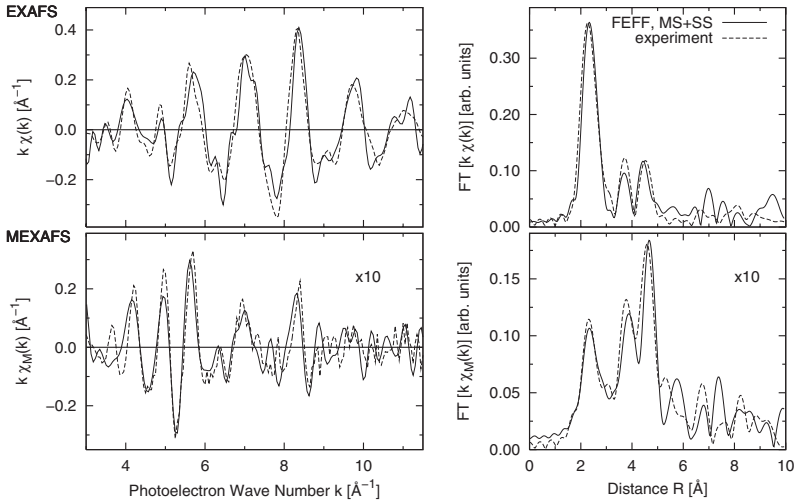

FIG. 3. *Ab initio* calculation with FEFF83 for the combined $L_{2,3}$ edges in comparison to the experiment (80 K) for EXAFS (top) and MEXAFS (bottom). For details, see main text.

also visible in the FT, where the longer distance contributions ($R>3$ Å), especially the second and third peaks located at $R\approx 3.8$ and 4.7 Å, are enhanced compared to the first peak at $R\approx 2.2$ Å. The enhancement of multiple scattering contributions was discussed in a qualitative manner in Ref. 5. In contrast, in the present work, we analyzed this enhancement quantitatively by studying the individual scattering contributions (see below). We show that the differences between the EXAFS and MEXAFS signals are due to (i) the overlapping of the $L_{2,3}$ edges and (ii) the enhanced multiple scattering contributions. Apart from this, significant intensities for $R>6$ Å in the FT of $\chi(k)$ and $\chi_M(k)$ can be observed, which have been identified very clearly here. For the $\chi_M(k)$ data, an increased noise contribution can be detected at larger k values in Fig. 2. However, this noise does not affect the reproducibility of the peaks in the Fourier transform for the two temperatures even at distances larger than 6 Å. This indicates that these contributions indeed stem from scattering phenomena and are no artifacts of the increased noise.

The theoretical descriptions of EXAFS and MEXAFS are quite advanced. For the *ab initio* calculations, the FEFF83 code[16] was employed using a Fe bcc lattice with $a=2.8665$ Å in a cluster with radius $R=10$ Å. All paths with a scattering amplitude of at least 3.5% relative to the nearest neighbor scattering contribution and a maximum of four scattering atoms were considered. The experimental signal is a superposition of the L_3 and L_2 edges. An electron originating from the $2p_{1/2}$ level (L_2) differs in energy from the one being excited from the $2p_{3/2}$ level (L_3) according to the spin-orbit splitting. So the absorption coefficient of the L_2 edge can be expressed as $\chi_{L2}(E)=\alpha\chi_{L3}(E+\Delta E_{SO})$, where $\Delta E_{SO}=-13.1$ eV. The energy shift has to be negative since an L_2 electron has less kinetic energy than a corresponding L_3 electron at a specific photon energy. The total absorption is then given by[18]

$$\chi_{L23}(E)=\frac{2}{3}[\chi_{L3}(E)+\alpha\chi_{L3}(E+\Delta E_{SO})], \tag{3}$$

with $\alpha=1/2$ for EXAFS and $\alpha=-1$ for MEXAFS according to a different transition probability and spin polarization at the two edges. This calculation is an ideal theoretical approach because it calculates the multiple scattering process in a given real crystallographic lattice. Another possibility is to perform a fitting procedure to the experimental data in k space and to extract information from the fit parameters, like recently done for Fe/V(110) by Rossner *et al.*[17] In the present work, we will focus on contributing scattering paths in both normal potential and spin-resolved scattering

A. Extended x-ray absorption fine structure

In Fig. 3, the experimental data are compared to *ab initio* calculations, confirming a bcc structure for the Fe film. We shall first focus on the EXAFS data. The frequency and enveloping intensity of $\chi(k)$ are reproduced quite well by theory. However, in the FT, there are some discrepancies between experiment and theory for $R>5$ Å. So the scattering-path analysis is only done for paths with $R_{\text{eff}}\leqslant 5.05$ Å. The required information to identify various scattering paths contributing to the EXAFS signal can be found in the intensity and position of the related peaks in the FT. In contrast to earlier investigations,[18] the contributions of all scattering paths are calculated separately. This is necessary to determine the peak maximum R correctly, which differs from

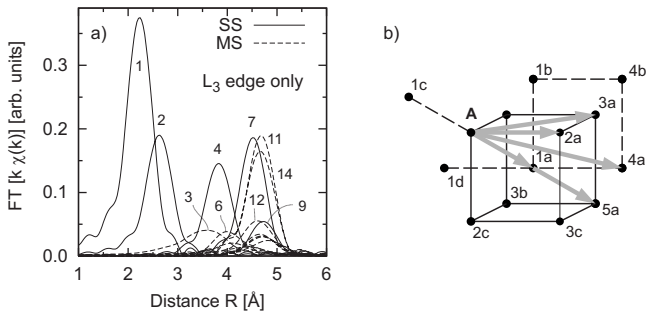

FIG. 4. (a) Scattering contributions to the EXAFS Fourier transform determined from FEFF calculations for the single Fe L_3 edge and (b) a schematic representation of the Fe lattice to describe the scattering paths. The numbers in the graph correspond to the scattering paths listed in Table I.

TABLE I. The 17 most important scattering paths to describe the EXAFS in bcc Fe up to R_{eff}=5.05 Å. Here, the ratio is the scattering amplitude relative to the first single scattering path, $\tilde{R}$ is the phase shifted peak maximum, and degeneracy D is the number of equivalent paths. The path types include "SS" single scatterings, "focusing" paths with only forward scattering events except for one backscattering, and "linear" collinear paths with more than one backscattering event.

Path	n shell	Ratio	D	R_{eff} (Å)	$\tilde{R}$ type (Å)
1	2 $A-1a-A$	100.00	8	2.48	2.24 SS, first shell
2	2 $A-2a-A$	53.80	6	2.87	2.63 SS, second shell
3	3 $A-1a-2a-A$	18.30	42	3.92	3.58 triangular
4	2 $A-3a-A$	55.26	12	4.05	3.83 SS, third shell
5	3 $A-1b-1d-A$	11.27	24	4.51	4.10 triangular
6	3 $A-1a-3a-A$	20.90	48	4.51	4.00 triangular
7	2 $A-4a-A$	78.17	24	4.75	4.51 SS, fourth shell
8	3 $A-2a-3a-A$	5.86	48	4.89	4.41 triangular
9	2 $A-5a-A$	23.55	8	4.96	4.72 SS, fifth shell
10	3 $A-1a-1c-A$	10.33	8	4.96	4.66 linear
11	3 $A-5a-1a-A$	66.69	16	4.96	4.68 focusing
12	4 $A-1a-A-1b-A$	14.42	8	4.96	4.60 dogleg
13	4 $A-1a-A-1a-A$	5.50	8	4.96	4.57 linear
14	4 $A-1a-5a-1a-A$	54.43	8	4.96	4.65 focusing
15	3 $A-1c-2a-A$	17.12	48	5.05	4.82 triangular
16	3 $A-4b-1b-A$	21.57	48	5.05	4.71 triangular
17	3 $A-4b-2a-A$	22.12	48	5.05	4.70 triangular

the effective path length R_{eff} due to the net scattering phase shift [see Eq. (1)]. To classify the various scattering paths, one distinguishes between single scattering (SS) and multiple scattering (MS) paths. As can be seen from Fig. 4(a), the main peak includes contributions from the nearest and next nearest neighbors. The two smaller peaks at $R \approx 3.8$ and 4.7 Å are related to longer path lengths including multiple scattering paths. In Table I, all paths are listed, which have been considered in the calculation. It is clear from Fig. 4 and Table I that the majority of peaks in the FT can be identified by SS paths only. However, some paths, namely, Nos. 11 and 14 can be identified as forward focusing ones. This confirms theoretical predictions (e.g., Ref. 19) and earlier experimental findings (e.g., Ref. 20). All other paths such as, e.g., the triangular ones at R=3.58 (No. 3) and 4.00 Å (No. 6) contribute much less. As we will see in the following section, this situation is different for magnetic scattering, where these paths also contribute significantly.

B. Magnetic extended x-ray absorption fine structure

Now we turn the attention to the MEXAFS data. In the *ab initio* calculation, the MEXAFS effect is explained by introducing an additive exchange contribution to the complex multiple Coulomb scattering expansion formalism. The lower part of Fig. 3 shows the MEXAFS calculation along with the experiment recorded at 80 K. The overall structure of the experimental $\chi(k)$ and most of the fine structures are reproduced reasonably well. In the FT, the enhancement of the second and third peaks with respect to the first peak is also reproduced.

As mentioned earlier, this enhancement is related to the relatively large amplitude of $\chi_M(k)$ in the range of the high frequency oscillation at $k<6$ Å^{-1} compared to the EXAFS $\chi(k)$. As described by Eq. (2) and observed by Srivastava *et al.*,[21] the enhancement in intensity of the second and third FT peaks can be partly attributed to MS contributions. To investigate this, we calculate the SS contributions separately. As can be seen from Fig. 5(a), in this k range, there are major multiple scattering contributions. In the FT [Fig. 5(b)], contributions from MS and SS are significantly different for the second and third peaks. In addition, the overlapping of the $L_{2,3}$ edges also influences the intensity of these peaks. This can be understood in the following manner: The (M)EXAFS signals $\chi_{L3}(E)$ and $\chi_{L2}(E)$ of the separate edges are basically identical except their threshold energy E_0 and a factor α [see Eq. (3)]. The energy difference shifts the L_2 spectrum such that in the high frequency range ($E-E_0<137$ eV), the oscillation $\chi_{L2}(E)$ is in antiphase with $\chi_{L3}(E)$. Hence, for a positive α (EXAFS), there is destructive interference, and for a negative α (MEXAFS), there is constructive interference. Since a high frequency oscillation in $\chi(k)$ corresponds to a long distance in the FT, this explains the enhanced intensity of peaks at $R>3$ Å with respect to the first peak in the FT of the MEXAFS data.

To disentangle the effects of MS contributions from the overlapping of $L_{2,3}$ edges, we compare the relative intensities in the Fourier transforms of the L_3 EXAFS, L_3 MEXAFS, and $L_{2,3}$ MEXAFS each by considering SS and MS+SS contributions (see Fig. 6). As expected, the superposition of the two edges enlarges the intensity of peaks at $R>3$ Å for SS

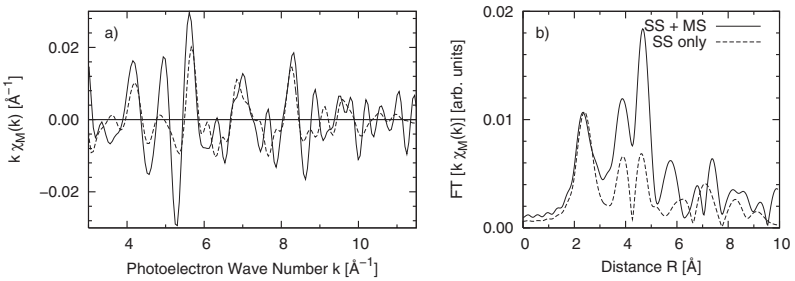

FIG. 5. *Ab initio* calculation of the MEXAFS for the combined $L_{2,3}$ edges. The solid line shows the single and multiple scattering contributions and is also plotted in Fig. 3. The dashed line shows a calculation, where only single scattering (SS) contributions are considered.

only [Fig. 6(a)] as well as for MS+SS [Fig. 6(b)]. However, the calculated FT for the separate L_3 edge is quasi-identical for EXAFS and MEXAFS when considering SS only. Hence, the magnetic scattering amplitude F_M scales the same for all SS paths compared to the Coulomb scattering amplitude F_C. Whereas when considering MS+SS, the intensity of peaks at $R>3$ Å is clearly enlarged, which now can only stem from MS contributions. This means that the *ab initio* calculation confirms Eq. (2) and in contrast to the scattering-path analysis done for EXAFS, where MS contributions play a minor role, for MEXAFS, they contribute significantly. As can be seen from Table I, these MS contributions are mainly triangular paths.

The spin-dependent scattering of the photoelectron can be modeled by the Coulomb potential describing the EXAFS signal. The spin up or down potential in this case is simulated by shifting the Coulomb potential in energy according for exchange interaction between the photoelectron and the scattering atoms. The rigid band model predicts an analogous spin-dependent energy shift ΔE of the density of states (DOS).[9,22] This energy shift is temperature dependent, since for randomly oriented spins ($T>T_C$), the magnetic interaction in each scattering process cancels out. Since the absorption coefficient is related to the empty DOS, one can calculate the MEXAFS spectrum from the experimental EXAFS spectrum just by shifting $\chi(E)$ in energy. Recently, this method has successfully been applied to the calculated EXAFS spectra for a Fe/V(110) system.[17] We have modeled MEXAFS spectra recorded at two different temperatures using this model with the experimental EXAFS spectra. The MEXAFS signal can be expressed by a simple subtraction of the energy-shifted spin-averaged absorptions yielding $\chi_M^{rb}(E,T)$ in the rigid band model:[10]

$$\chi_M^{rb}(E,T) = \chi\left(E - \frac{1}{2}\Delta E(T)\right) - \chi\left(E + \frac{1}{2}\Delta E(T)\right). \quad (4)$$

The energy shift ΔE is the only free parameter and scales the intensity. It is a direct measure for the local magnetic coupling, which is the quantity we are interested in. In Ref. 10, this model was applied to the experimental EXAFS data of a Gd single crystal. To account for the the overlap of the $L_{2,3}$ edges in a $3d$ transition metal, we assumed $\chi_{L23} \approx \chi_{L3}$ and extended Eq. (4) analog to Eq. (3),

$$\chi_{M,L23}^{rb}(E) = \chi_{M,L3}^{rb}(E) - \chi_{M,L3}^{rb}(E + \Delta E_{SO}). \quad (5)$$

Using our experimental $\chi(E)$ in Eqs. (4) and (5) yields the MEXAFS spectra shown in Fig. 7 with $\Delta E(300\ \mathrm{K}) = (0.77 \pm 0.05)$ eV and $\Delta E(80\ \mathrm{K}) = (0.80 \pm 0.05)$ eV. The agreement of experiment and this model is quite good even for distances $R>6$ Å in the FT. Hence, the magnetic EXAFS can indeed be described by the density of scattering states, which are energy shifted due to magnetic exchange coupling. This model is applied here for the temperature-dependent MEXAFS data of a $3d$ element. Thereby, the effect of spin fluctuations can be separated from lattice vibrations since the temperature dependence of $\Delta E(T)$ is only influenced by the spin fluctuations. It is to be noted that $\Delta E(T)$ is nearly constant as $M(T)$ does not change significantly in this temperature range (80–300 K) for a 13 ML Fe film. Therefore, the observed temperature dependence in the magnetic EXAFS is mainly due to a change in the Debye-Waller factor.

IV. CONCLUSION

The present work shows high quality EXAFS and MEXAFS data resulting in significant intensities for distances larger than 6 Å in the corresponding Fourier transforms. The detailed scattering-path analysis shows predominant intensi-

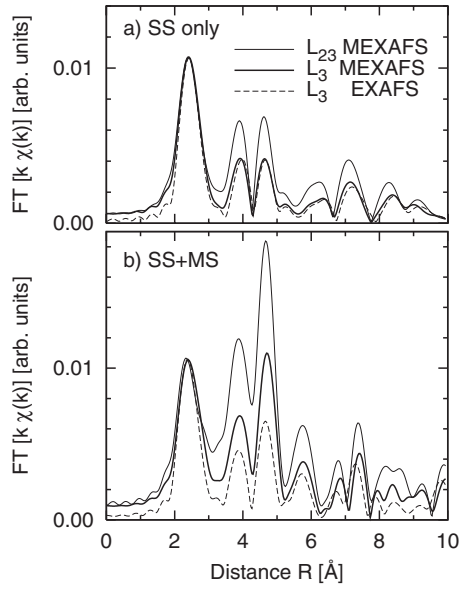

FIG. 6. Origin of the enhanced second and third peaks in the magnetic EXAFS. (a) The intensity of single scattering contributions is the same for EXAFS and MEXAFS at the separate L_3 edge, where in the full calculation (SS+MS), (b) a clear enhancement is there. The overlapping of the edges affects both single and multiple scattering contributions. The spectra were scaled to fit the first peak.

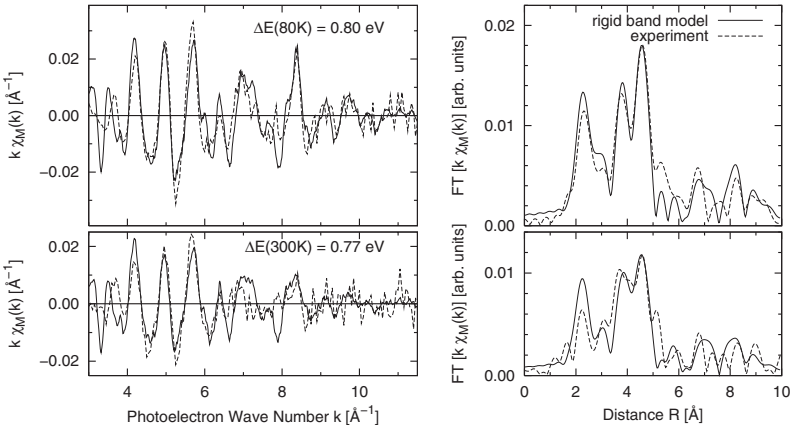

FIG. 7. Application of the rigid band model in comparison to the experimental data. The solid line spectra are calculated according to Eq. (5). Taking into account the simplicity of the model [Eqs. (4) and (5)], we achieved an amazing agreement with the experimental data, even for distances $R>6$ Å in the FT. The temperature-dependent damping is mainly due to lattice vibrations, since $\Delta E(T)$ is constant within the error of ±0.05 eV (see text).

ties for single and forward scattering in the case of EXAFS. Whereas in the case of MEXAFS, also triangular paths contribute significantly. This scattering-path analysis in real space gives a very specific insight into the microscopic traveling path of the photoelectron, i.e., its interaction with the nearest neighbor potentials, on an atomic scale. It is shown that the rigid band model works quite well to reproduce MEXAFS data, and the energy shift $\Delta E(T)$ is proportional to the sample magnetization. We have thus a powerful tool to separate spin fluctuations from lattice vibrations in the MEXAFS signal. In the future, it would be very interesting to study nearest neighbor coupling in the vicinity of Curie temperature with this method.

ACKNOWLEDGMENTS

This work is supported by BMBF (05 KS4 KEB 5) and DFG (Heisenberg-Stipendium). We thank H. H. Rossner for discussion of his FEFF calculations. One of us (P.S.) wishes to thank DFG (SFB 658) for financial assistance and University of Duisburg-Essen for hospitality and support.

*Permanent address: Department of Physics, IIT Delhi, Hauz Khas, New Delhi 110 016, India.
†Corresponding author. FAX: +49 (0)203 379 3601. heiko.wende@uni-due.de; URL: http://www.uni-duisburg.de/FB10/LAPH/Wende/

[1] G. Schütz, R. Frahm, P. Mautner, R. Wienke, W. Wagner, W. Wilhelm, and P. Kienle, Phys. Rev. Lett. **62**, 2620 (1989).
[2] M. Knülle, D. Ahlers, and G. Schütz, Solid State Commun. **94**, 267 (1995).
[3] E. Dartyge, F. Baudelet, C. Brouder, A. Fontaine, J. G. Kappler, G. Krill, C. Giorgetti, M. F. Lopez, and S. Pizzini, Physica B **208-209**, 751 (1995).
[4] G. Schütz and D. Ahlers, in *Spin-Orbit-Influenced Spectroscopies of Magnetic Solids*, edited by H. Ebert and G. Schütz, Vol. 466 of Lecture Notes in Physics (Springer, Berlin, 1996), p. 229.
[5] D. Ahlers and G. Schütz, Phys. Rev. B **57**, 3466 (1998).
[6] A. L. Ankudinov and J. J. Rehr, Phys. Rev. B **56**, R1712 (1997).
[7] H. Ebert, V. Popescu, and D. Ahlers, Phys. Rev. B **60**, 7156 (1999).
[8] Ch. Brouder and M. Hikam, Phys. Rev. B **43**, 3809 (1991).
[9] Ch. Brouder, M. Alouani, and K. H. Bennemann, Phys. Rev. B **54**, 7334 (1996).
[10] H. Wende, Rep. Prog. Phys. **67**, 2105 (2004).
[11] H. Wende, J. W. Freeland, V. Chakarian, Y. U. Idzerda, L. Lemke, and K. Baberschke, J. Appl. Phys. **83**, 7028 (1998).
[12] M. Stampanoni, A. Vaterlaus, M. Aeschlimann, and F. Meier, Phys. Rev. Lett. **59**, 2483 (1987).
[13] A. Hahlin, C. Andersson, J. H. Dunn, B. Sanyal, O. Karis, and D. Arvanitis, Phys. Rev. B **73**, 134423 (2006).
[14] M. Newville, P. Livins, Y. Yacoby, J. J. Rehr, and E. A. Stern, Phys. Rev. B **47**, 14126 (1993).
[15] For details see page 253 of Ref. 4.
[16] A. L. Ankudinov, C. E. Bouldin, J. J. Rehr, J. Sims, and H. Hung, Phys. Rev. B **65**, 104107 (2002).
[17] H. H. Rossner, D. Schmitz, P. Imperia, H. J. Krappe, and J. J. Rehr, Phys. Rev. B **74**, 134107 (2006).
[18] H. Wende, P. Srivastava, D. Arvanitis, F. Wilhelm, L. Lemke, A. L. Ankudinov, J. J. Rehr, J. W. Freeland, Y. U. Idzerda, and K. Baberschke, J. Synchrotron Radiat. **6**, 696 (1999).
[19] E. A. Stern, *X-ray Absorption: Principles, Applications, Techniques of EXAFS, SEXAFS, and XANES* (Wiley-Interscience, New York, 1988).
[20] S. I. Zabinsky, J. J. Rehr, A. L. Ankudinov, R. C. Albers, and M. J. Eller, Phys. Rev. B **52**, 2995 (1995).
[21] P. Srivastava, L. Lemke, H. Wende, R. Chauvistré, N. Haack, K. Baberschke, J. Hunter-Dunn, D. Avernitis, N. Mårtensson, A. Ankudinov, and J. J. Rehr, J. Appl. Phys. **83**, 7025 (1998).
[22] J. L. Erskine and E. A. Stern, Phys. Rev. B **12**, 5016 (1975).